Brief sleep disruption following hippocampus-dependent learning downscales interneuron synapses within lateral entorhinal cortex

Abbreviated title: Sleep loss and neocortical interneurons

Authors and affiliations: Vinodh Balendran[1], Jiyang Liu[1], Katelin Wu[1], Sara J. Aton[1*]

[1] Department of Molecular, Cellular, and Developmental Biology, University of Michigan, Ann Arbor, MI 48019

[*] **Corresponding author email:** saton@umich.edu

Conflict of interest statement: The authors declare no competing financial interests.

Acknowledgements: Schematic figures were created using BioRender. This work was supported by NIH research grants R01NS118440 and R01MH135565 and a Chan Zuckerberg Initiative Collaborative Pairs Grant to S.J.A.

Financial Disclosure: The authors have no financial conflicts of interest.

Non-Financial Disclosure: The authors have no non-financial conflicts of interest.

Abstract

Study objectives: Brief sleep loss alters cognition and the activity and synaptic structures of both principal neurons and interneurons in hippocampus. However, although sleep-dependent coordination of activity between hippocampus and neocortex is essential for memory consolidation, much less is known about how sleep loss affects neocortical input to hippocampus, or excitatory-inhibitory balance within neocortical structures. We aimed to test how the synaptic structures of SST+ interneurons in lateral and medial entorhinal cortex (LEC and MEC), which are the major neocortical input to hippocampus, are affected by brief sleep disruption in the hours following learning.

Methods: We used Brainbow 3.0 to label SST+ interneurons in the LEC or MEC of male *SST-IRES-Cre* transgenic mice. We then compared synaptic structures in labeled neurons after single trial contextual fear conditioning (CFC) followed by either a 6-h period of *ad lib* sleep, or gentle handling sleep deprivation (SD), focusing on cortical layers providing input to hippocampus.

Results: Dendritic spine density among EC SST+ interneurons was altered in a subregion-specific manner, with dramatic alterations in dendritic spine type distributions and reductions in spine size in LEC, but not MEC, after post-CFC SD.

Conclusions: Our data suggest that the synaptic connectivity of SST+ interneurons is significantly reduced in LEC when learning is followed by sleep disruption. This suggests that post-learning sleep loss disrupts hippocampus-dependent memory processing in part through altered excitatory-inhibitory balance in neocortical structures providing input to hippocampus. They also provide more mechanistic insight into sleep's role in coordinating neocortical-hippocampal communication in the context of memory consolidation.

Keywords:

Interneuron, synaptic plasticity, sleep deprivation, hippocampus, neocortex, synaptic structure, excitatory-inhibitory balance

Significance Statement

Changes to the function of somatostatin-expressing (SST+) interneurons have been implicated in the etiology of psychiatric and neurological disorders in which both cognition and sleep behavior are affected. Here, we measure the effects of very brief experimental sleep deprivation on synaptic structures of SST+ interneurons in entorhinal cortex - a brain structure that provides input

to the hippocampus and is critical for sleep-dependent memory processing. We find that only six hours of post-learning sleep deprivation restructures SST+ interneurons' dendritic spines, causing dramatic, subregion-specific reductions in dendritic spine size. These changes have the potential to dramatically alter excitatory-inhibitory balance gating neocortical input to hippocampus, leading to cognitive disruptions commonly associated with sleep loss.

Introduction

Mental health and cognition are severely impacted by sleep quantity and quality. Even just a few hours of sleep deprivation (SD) can impair cognitive performance in both humans and animal models, although the underlying neurobiological mechanisms are poorly understood [1-5]. Growing evidence also suggests that sleep disruption (i.e., more chronic SD) occurs prior to cognitive and/or behavioral changes in psychiatric and neurological disorders such as schizophrenia, bipolar disorder, and Alzheimer's disease [6-13]. An intriguing link between SD and the etiology of neuropsychiatric disorders is disrupted somatostatin-expressing (SST+) interneuron activity. Loss of function in this and other inhibitory neuron populations has been identified at the early stages of these disorders' progression [14-17]. Recent studies have from our lab and others have indicated that SST+ interneurons in the hippocampus are selectively activated by SD [18-20]. This activation contributes to both the disruption of hippocampus-dependent memory consolidation and the inhibition of principal cell activity in the context of memory processing [18,21-23]. For example, consolidation of contextual fear memory (CFM) is disrupted by post-learning SD in part via effects on hippocampal SST+ interneuron populations [18]. Our lab has shown that SST+ interneuron synaptic structures are dramatically altered by SD in the dorsal hippocampus, as well as in medial prefrontal and primary visual cortices [22]. These changes – for example, dramatic increases in interneurons' dendritic spine size in hippocampal CA3 and increases in spine density in CA1 – support the idea that SD can increase network inhibition within the hippocampus, leading to cognitive disruption.

The entorhinal cortex (EC) serves as the primary functional and anatomical interface between the hippocampus and various neocortical regions. Principal neurons in the EC's superficial layers providing the primary cortical input to the hippocampus relative to the deep layers via both the perforant and temporoammonic pathways [24-28]. These excitatory inputs to hippocampus mediate information transfer during memory processing and modulate hippocampal synaptic plasticity. The EC also receives the major output from the hippocampus, via the CA1 and subiculum. These bidirectional connections between EC and hippocampus are critical for the encoding, consolidation, and retrieval of spatial and episodic memories [24,25,29,30].

The EC comprises two major subdivisions - medial and lateral. The medial entorhinal cortex (MEC) is largely reciprocally connected with spatial processing regions of the brain, receiving inputs from structures such as the retrosplenial cortex and dorsal presubiculum [31,32]. Meanwhile, the lateral entorhinal cortex (LEC) is thought to encode non-spatial information

including temporal associative memory and object recognition [33-35]. Because of the important roles that both LEC and MEC play in memory processing, an unanswered question is how the activity and function of these structures are affected by brief periods of SD, which are sufficient to disrupt memory processing at multiple stages [36-40]. Recent studies have shown that SD following learning impacts both neocortical synaptic plasticity and neocortex-dependent memory [41-48]. However, the majority of these studies have focused on principal neurons, and far less is known about how neocortical interneurons are affected by sleep loss. Moreover, while some studies have identified effects of post-learning sleep disruption on synaptic structures in neocortical principal neurons [41,49], it is unclear whether interneurons are similarly affected by post-learning sleep loss. We hypothesized that the structure and function of SST+ interneurons in LEC and MEC might be affected by post-learning SD in a manner similar to the hippocampus or other cortical structures [18,22]. To investigate how the structure of SST+ interneurons in these regions were affected by SD, we used Cre-dependent Brainbow 3.0 labeling of EC interneurons to assess their dendritic and synaptic morphologies following learning followed by brief periods of SD vs. *ad lib* sleep. We find that EC SST+ interneurons show profound alterations in spine structure following 6 h of post-learning SD. These changes occur in a subregion-specific manner, with LEC SST+ interneurons' dendritic spines being dramatically affected by SD (with significant reductions in spine volume, surface area, and backbone length), and MEC interneurons being largely unaffected. These data provide new insights into how the major input to hippocampus is affected by post-learning SD, as well as how SD can dramatically impact inhibitory networks within the neocortex. They also provide further evidence of the diversity of SD-mediated changes to neocortical circuits, with effects that are cell type-, microcircuit-, and brain region-specific [21,22,50,51].

Materials and Methods

Mouse husbandry: *SST-IRES-CRE* mice on a C57Bl6/J genetic background (JAX) were group-housed on a 12 h light/12 h dark cycle (lights on 9:00 AM – 9:00 PM) and under constant temperature (22 ± 2°C), with *ad libitum* food and water access, in standard transparent filter-top caging. Following post-operative recovery from transduction procedures see below) mice were single housed with multiple forms of nesting material as beneficial enrichment. SD and sleep monitoring was carried out in each mouse's home cage. All animal husbandry and experimental procedures were approved by the University of Michigan Institutional Animal Care and Use Committee (IACUC).

AAV-mediated Brainbow labeling of SST+ interneurons: At age 4-15 months (LEC Sleep: 8.1 ± 1.7 months; SD: 7.4 ± 2.0 months; MEC Sleep: 11.4 ± 1.4 months; MEC SD: 11.4 ± 1.7 months), *SST-IRES-CRE* male mice were transduced under isoflurane anesthesia with a cocktail of CRE recombinase-dependent AAV vectors to drive expression of Brainbow 3.0 (AAV-EF1a-BbTagBY and AAV-EF1a-BbChT; titers ≥ 1×10^{13} vg/mL; Addgene) [52] in EC structures. 2 µL of this AAV cocktail was delivered bilaterally to either LEC or MEC using the following stereotaxic coordinates: LEC: A/P -3.5 mm, M/L ±3.75, D/V -4.5 mm; MEC: A/P -4.5, M/L ±3.6 mm, D/V -4.25 mm.

Handling, contextual fear conditioning (CFC), and sleep deprivation (SD): Following transduction procedures, each mouse was allowed 9 days of postoperative recovery, after which they were single housed for 5 subsequent days of habituation to handling procedures. Each mouse was handled for 5 min/day for 5 days preceding experimentation. Following habituation, all mice underwent single-trial contextual fear conditioning (CFC) at ZT0 (lights-on), in which they were placed in a novel conditioning chamber (Med Associates) and allowed 2.5 minutes of free exploration followed by a single 2-s, 0.75 mA foot shock through the chamber's grid floor. After 3 minutes total in the conditioning chamber, mice were returned to their home cage. Mice in the control group were allowed *ad lib* sleep while mice in the experimental group underwent 6 h of SD by gentle handling (where arousals from sleep were achieved via cage tapping, cage shaking, and gentle nest disturbance without the introduction of novel stimuli). This duration and method of post-CFC sleep deprivation has been shown to consistently disrupt consolidation of contextual fear memory (CFM) in mice [37-40,53]. The necessity of interventions (to disrupt sleep attempts) were documented, and the increasing frequency over the course of the 6-h period confirmed increases in sleep pressure over the course of deprivation. Mice allowed *ad lib* sleep were monitored visually in 5-min increments to quantify sleep behavior (i.e. assumption of characteristic sleep postures, with closed eyes and immobility) in the home cage. This method of sleep quantification has been validated for accuracy, providing quantitative total sleep measures comparable with polysomnographic sleep measurement [54].

Tissue harvest and immunohistochemistry: Immediately following the 6-h *ad lib* sleep or SD period, mice were euthanized via an overdose of pentobarbital and were perfused transcardially with ice cold PBS followed by 4% paraformaldehyde for brain tissue harvest. Perfused brains were post-fixed for 24 h in 4% paraformaldehyde at 4°C, washed with PBS, and sectioned

coronally (80 μm thickness) using a vibratome. Free floating brain sections were blocked overnight at 4°C in PBS containing 5% normalized goat serum and 1% Triton X-100.

Perfused brains were post-fixed for 24 h in 4% paraformaldehyde at 4°C, washed with PBS, and sectioned coronally (80 μm thickness) using a vibratome. This section thickness was chosen to maximize the extent of dendrite sampling in the Z-plane, without compromising our ability to resolve dendritic spines (i.e., due to light scatter) [52,55]. Free floating brain sections were blocked overnight at 4°C in PBS containing 5% normalized goat serum and 1% Triton X-100. Each section was then incubated for 72 h at 4°C in PBS with 5% normal goat serum, 0.5% Triton X-100 and the following primary antibodies chicken anti-EGFP, rat anti-mTFP, and guinea pig anti-TagRFP (all at 1:1000). Following three 1-h rinses at room temperature in PBS with 1% normal goat serum and 0.5% Triton X-100, sections were incubated for 72 h at 4°C in PBS with 5% normal donkey serum, 0.5% Triton X-100 and the following secondary antibodies: goat anti-chicken Alexa Fluor 488, goat anti-rat Alexa Fluor 555, and goat anti-guinea pig Alexa Fluor 633 (all 1:1000). After secondary antibody incubation, sections received three 1-h rinses and were cover slipped using ProLong Gold antifade mounting medium (ThermoFisher Scientific).

Imaging, 3D reconstruction of dendritic arbors, and morphological metrics: Images of Brainbow-labeled neurons were acquired using an SP8 confocal microscope (Leica Microsystems) with a 40x oil-immersion objective lens, as described previously [22]. Images spanned at least 40 μm in depth, using 0.3 μm acquisition steps. Full Z-stack images (0.189 μm/voxel in the X and Y planes, 0.3 μm Z steps) were exported using LAS X software (Leica Microsystems) and traced using Neurolucida360 (MBF Bioscience). Similar results (in terms of numbers of detected spines per dendrite, and their categorization into different spine types) were obtained for images taken at a higher (63x) magnification. For each transduced brain region and animal, Brainbow-labeled neurons with the most complete dendritic arbors represented within the Z-stack (i.e., with no cropping of dendrites within the X and Y planes, and the most complete sampling across the Z plane) were identified. Of those neurons with fully-imaged dendritic arbors, 4–5 were selected at random within each region for 3D reconstruction. Somas were detected automatically (with detection sensitivity varying between 70–100% depending on the signal contrast and intensity), and dendritic arbors were semi-automatically traced. Neurons were selected for analysis with the aim of limiting truncation of dendritic arbors; where dendrites were truncated at a length ≤ 10 μm, these dendrites were excluded from subsequent analysis. Dendritic spines were automatically detected along the full length of traced dendrites, using the following

settings: outer range between 1.5 and 3 μm, a minimum height of 0.3 μm, and detector sensitivity set between 75 and 120 μm. Using Neurolucida 360's preset definitions, spine morphology was classified automatically into one of 4 classes: mushroom, stubby, thin, or filopodium [56,57]. The criteria for assigning spines to a specific class are based on prior work quantifying morphology of principal neurons, where spine head diameter/neck diameter ratios, backbone length/head diameter ratios, overall backbone length, and overall head diameter are used for classification [58]. Each spine's location along the dendrite was used to calculate overall spine density. Within each class of spine, surface area and volume parameters were used for subsequent analysis. Spine surface area was defined as the apparent exterior surface area of the spine (in μm^2). Spine volume was calculated as the number of voxels that make up the spine object multiplied by the volume of a single voxel (in μm^3).

Statistical analyses: Experimenters were blinded to animal treatment conditions throughout image analyses. Data analyses and generation of summary figures were carried out using GraphPad Prism10 (v10.5.0). Statistical comparisons of interventions needed to maintain wakefulness during SD were made between groups using a weighted measure, aggregated across the entire 6-h SD period. For this, individual interventions were weighted based on the intensity of the delivered stimulus, where cage taps were scored as 1, cage shakes as 2, and nest disturbance as 3.

To examine the relative proportion of spine types on SST+ interneurons measured in the Sleep and SD groups (n=5 animals per group) the percentages of each animal's total detected spines belonging to each spine type were compared using Welch's t-test. The same statistical test was used to compare the percentage of spine types expressed in the Sleep and SD groups. Spine density was assessed using nested t-tests wherein density values from interneurons imaged from the same animal were grouped together within either the Sleep or SD experimental groups. Cumulative distributions of individual spine characteristics (spine volume, surface area, and backbone length) were compared between the Sleep and SD groups using unpaired Kolmogorov-Smirnov (KS) tests.

Results

Post-learning SD differentially affects the types of dendritic spines on MEC and LEC SST+ interneurons

To characterize morphology in EC SST+ interneurons, *SST-IRES-CRE* mice were transduced with AAV vectors to express Brainbow 3.0 in a CRE recombinase-dependent manner in either LEC or MEC [52]. Following postoperative recovery and habituation to daily handling, all mice underwent single-trial CFC at lights on (ZT0). Following CFC, each mouse was returned to their home cage for either 6 h of *ad lib* sleep (control condition) or sleep deprivation (SD) by gentle handling (a manipulation that is sufficient to disrupt CFM consolidation)[37-40] (**Figure 1A, left**). All mice were then perfused for MEC or LEC SST+ interneuron imaging and morphological analysis (**Figure 1A, right**).

Ad lib sleep behavior was visually monitored and quantified in control mice. LEC- and MEC-transduced control mice spent similar proportions of the 6-h period asleep (66.11% ± 3.12% vs. 62.78% ± 3.44%, respectively; p = 0.675, nested t-test) and had similar sleep bout numbers and mean bout durations (p = 0.873 and 0.827, respectively, Nested t-test) (**Figure 1B**). The frequency and type of gentle handling interventions required to maintain wakefulness in SD mice was also similar between LEC- and MEC-transduced groups (p = 0.07, Welch's t-test) (**Figure 1C**). Mice in both SD groups exhibited apparent increases in sleep pressure across the 6-h period of SD, as evidenced by the increased frequency of interventions (cage taps, cage shakes, nest disturbances) required to keep mice awake over time.

Brain sections from control and SD mice were immunolabeled and imaged for 3D reconstruction of Brainbow-labeled SST+ interneurons (*n* = 4-5 neurons per region per animal). Dendritic arbors of interneurons with somata in MEC and LEC layers 2 and 3 (corresponding to EC layers receiving input from cortex and sending output to hippocampus [25,27,28] were traced and reconstructed in a semi-automated manner for subsequent spine detection along their length (**Figure 1A, right**). Based on morphological parameters previously used to characterize dendritic spines in principal neurons [22,58], individual dendritic spines were categorized as thin, stubby, mushroom, or filopodia. The overall distribution of these spine types in LEC and MEC were similar to those found on SST+ interneurons in other brain regions, including other cortical structures (i.e. medial prefrontal and primary visual cortices) [22]. In freely sleeping control mice, thin and stubby spines made up the majority of total spines in both MEC and LEC, although the relative proportion of these two spine types differed between regions. In LEC Sleep mice, thin spines (which are transient and very plastic [59]) were more numerous, accounting for 42.6% of total spines (n = 1968 spines from 25 interneurons measured from 5 mice). Stubby spines accounted for an additional 37.0%, and mushroom spines and filopodia made up the remaining 18.8% and 1.6%, respectively.

In MEC Sleep mice, stubby spines were most prevalent, making up 50.8% of total spines (n = 2899 spines from 25 interneurons measured across 5 mice) followed by thin spines (29.3%), mushroom spines (19.1%), and filopodia (0.9%).

Interneurons' spine type distributions were significantly altered by SD in LEC. After SD, the proportion of total spines with stubby morphology increased from 37% to over 66% in the SD group (n = 2275 spines from 24 interneurons measured from 5 mice) (**Figure 2A**). When spine type proportions were compared across individual mice, this led to a significant difference in stubby spine proportions between the two groups (Sleep stubby spines = 37.6% ± 7.9%, SD stubby spines = 61.5% ± 6.6%, Welch's t-test, p = 0.05). This increase was primarily offset by a trend for decreased thin spine representation in LEC (Sleep thin spines = 42.7% ± 8.4%, SD thin spines = 23.6% ± 2.53%, Welch's t-test, p = 0.08). The remaining spine types also showed slight changes after SD. While mushroom spine distributions in LEC were not significantly affected (Sleep mushroom spines = 18.1% ± 2.9%, SD mushroom spines = 14.6% ± 0.4%, Welch's t-test, p =0.52), the proportion of spines with filopodia morphology was reduced by SD (Sleep filopodia spines = 1.7% ± 0.4%, SD filopodia spines = 0.3% ± 0.1%, Welch's t-test, p = 0.02). While overall spine density in LEC interneurons was unaffected by SD (**Figure 2B**), SD decreased density of filopodia (nested t-test, p <0.05), consistent with the observed changes in filopodial representation between groups. Because stubby spines and filopodia are thought to represent transient states in the process of excitatory synapse elimination and formation, respectively [56,57,60], these data suggest that in LEC, brief SD may selectively promote elimination and suppress formation of excitatory inputs to SST+ interneurons.

In contrast to the clear effects of SD on dendritic spine morphology in LEC, spine type distributions were unchanged in MEC SST+ interneurons after SD (n = 2251 spines from 25 interneurons measured from 5 mice) (**Figure 2A**). While an overall 5.4% reduction in thin spine representation was observed after SD (from 29.3% in freely sleeping mice to 23.9%), assessing type distributions across individual mice revealed no significant changes. For example, stubby spine and filopodia proportions were nearly identical between control and SD mice (Sleep stubby spines = 49.0% ± 8.8%, SD stubby spines = 51.3% ± 7.4%, Welch's t-test, p =0.85; Sleep filopodia spines = 0.9% ± 0.2%, SD filopodia spines = 1.0% ± 0.2%, Welch's t-test, p =0.79). Mushroom and thin spine proportions were similarly unaffected by SD (Sleep mushroom spines = 18.7% ± 1.7%, SD mushroom spines = 23.3% ± 4.0%, Welch's t-test, p =0.35; Sleep thin spines = 31.4% ± 10.2%, SD thin spines = 24.5% ± 7.7%, Welch's t-test, p =0.61). Consistent with the lack of changes in spine morphologies, overall spine density was unchanged in MEC after SD (**Figure**

2B), with density of all spine types unchanged between sleep and SD mice. Together, these data suggest that 6 h of post-CFC SD is sufficient to alter distributions and densities of some spine types in LEC SST+ interneurons, but has no effect on MEC interneuron populations.

SST+ interneurons' dendritic spine morphologies are differentially altered by post-learning SD in LEC and MEC

Previous research has shown that SD can alter the size and shape of individual dendritic spines on both principal neurons and interneurons in both hippocampus and neocortex [22,61-63]. Because we observed differential effects of post-CFC SD on spine type distributions in LEC vs. MEC, we next tested whether SD differentially alters spine surface area and volume in interneurons from the two structures. In the LEC, SD led to an overall decrease in the volume of individual spines (Kolmogorov-Smirnov test, $p<0.0001$) (**Figure 3A**). This effect was observed for both mushroom and stubby spine subclasses (Kolmogorov-Smirnov test, $p<0.0001$), while thin and filopodia spines' volumes were not significantly affected by SD. Similarly, SD led to a general decrease in spine surface area in LEC interneurons (Kolmogorov-Smirnov test, $p<0.0001$) (**Figure 3B**), which significantly impacted mushroom ($p<0.0001$), thin ($p<0.05$), and stubby ($p<0.0001$) spine classes. Finally, we assessed backbone length, as a third metric of spine size. SD decreased backbone length across all spine types (Kolmogorov-Smirnov test, $p<0.0001$) as well as in thin ($p<0.0001$) and stubby ($p<0.0001$) spine subtypes (**Figure 3C**). These data indicate that in LEC SST+ interneurons, SD decreases the overall size of virtually all spines - including types that undergo no changes in distribution or density. Together, these findings support the notion that SD causes dramatic synaptic downscaling within this inhibitory interneuron population in LEC.

In striking contrast to the dramatic changes observed in LEC interneurons after SD, we observed no significant changes in either overall or subtype-specific spine volume distributions in MEC interneurons (**Figure 4A**). Similarly, we found no significant changes in MEC interneurons' spine surface areas after SD (**Figure 4B**). Finally, as shown in **Figure 4C**, MEC interneurons' spine backbone lengths were also generally unaffected by SD - except for a small but significant *increase* in the backbone length of MEC mushroom spines (Kolmogorov-Smirnov test, $p<0.05$). Thus, while we find substantial evidence of dendritic spine downscaling in LEC SST+ interneurons after SD, there is no evidence of downscaling for this same interneuron population in MEC. Because previous studies indicate a link between dendritic spine size and excitatory synapse

strength [60,64,65], our findings therefore suggest that 6 h of post-CFC SD substantially reduces total excitatory input to interneurons in LEC, but not MEC.

Discussion

Our data show that SST+ interneurons in EC structures can be altered substantially by 6 h of post-learning SD - a sleep manipulation that disrupts the consolidation of CFM. More specifically, we find that multiple dendritic spine types in LEC, but not MEC, interneurons are substantially reduced in size after SD. While the overall interneuron spine density in these regions is unaffected by SD, the distribution of spine types in LEC is also altered by SD, with increased representation of stubby spines and decreased representation of filopodia. These data build on our previous findings that SD alone (without prior learning) affects dendritic spine density and size among SST+ inhibitory networks in dorsal hippocampus and neocortex [22].

Our present findings raise the question: what is the functional consequence of these SD-driven structural changes for synaptic function in SST+ interneurons? The structural plasticity of dendritic spines is known to be associated with changes to postsynaptic densities (PSDs) [66]. For example, spine head size is proportional to that of the PSD, as well as both the number of postsynaptic receptors and presynaptic docked vesicles [57]. Long-term potentiation (LTP) at glutamatergic synapses is sufficient to enlarge dendritic spines - or promote new spine formation - in a variety of brain regions, while long-term depression (LTD) promotes shrinkage or elimination of spine heads [66,67]. These changes in synapse number and strength are thought to provide a mechanism for *de novo* memory formation [65]. Critically, spines on neocortical pyramidal dendrites have greater long-term stability than those on hippocampal pyramidal neurons [68,69], which may provide optimal conditions for longer-term - even lifelong - memory storage in neocortex [70]. Morphologically defined spine types are generally regarded as an indicator of dendritic spines' maturity and stability (from least- to most-stable, spines classified as either filopodia, thin, stubby, or mushroom) [57,59,71,72]. Spine type transitions are common in the context of synaptic strength changes [73]. For example, stubby spines may reflect the retraction or shrinkage of mature mushroom spines in the context of spine elimination [74], or simply a less structurally and functionally mature spine type [75]. While most of our understanding of the structure-function relationship of dendritic spines comes from analysis of principal neurons, available data suggest that dendritic spines on SST+ interneurons, similarly, represent postsynaptic contact sites for

glutamatergic synapses, with similar dendritic spine type morphologies, plasticity, and synapse characteristics as those of principal neurons [76].Thus, we interpret our current and recent findings [22] as reflecting SD-driven changes in excitatory input onto inhibitory interneurons within brain circuits, which is likely to in turn drive changes in network inhibitory neurotransmission.

The EC is thought to be critical for both initial acquisition and retrieval of hippocampus-dependent memories [24], and continues to mediate remote memory retrieval even after the hippocampus is no longer required [24,77]. EC input to hippocampus (e.g. from neurons in layers 2 and 3) provides information about head direction and spatial location, as well as indirect input from the basolateral amygdala, which is essential for the acquisition of CFM [78-81]. Within the EC, SST+ interneurons support the spatial information coding of neighboring principal neurons [82]. Thus, the changes to synapses we observe in EC SST+ interneurons after SD are likely to have important consequences for both local EC and hippocampal information processing following CFC.

Another unanswered question, based on our present findings, is: what is the cognitive consequence of SD-driven structural changes to interneurons occurring selectively within LEC (and not in MEC) in the hours following CFC? Inhibition of MEC activity immediately after CFC impairs CFM consolidation [83], and activity patterns in MEC appear to be instructive for consolidation, with sleep-dependent replay of neuronal firing patterns observed during prior learning occurring within the MEC superficial layers [84]. Similarly, offline reactivation of learning-activated engram neuron populations within superficial layers of LEC is essential for consolidating object-location-context associative memory [85]. The LEC's role in consolidation of CFM is less well understood, although CFC includes a temporal associative component that is generally attributed as an LEC function [31-35].

Both the changes we observe in LEC interneurons with SD, and lack of changes to interneurons in MEC, may have important consequences for CFM consolidation. Prior studies have shown that brief SD can reduce synaptic abundance of NMDA receptors in EC, as well as the GluA1 AMPA receptor subunits that mediate AMPA receptor trafficking to and from synaptic membranes [86]. Our general finding of spine shrinkage in LEC interneurons after SD is consistent with this finding, and suggests that at least some of these changes occur at excitatory synapses onto SST+ interneurons. While it remains unclear how principal neurons in LEC and MEC are affected by post-CFC SD, one possibility is that the selective structural changes we observe across LEC and MEC interneurons lead to altered excitatory-inhibitory balance in one or both

structures. For example, the apparent reduced excitatory input to LEC interneurons could lead to selective disinhibition of the LEC network. Further, if SD affects excitatory synapses on principal neurons in MEC, the lack of change to the SST+ interneuron network would be associated with either a relative increase, or decrease, in network inhibition. Critically, the LEC projects preferentially to the superior blade of hippocampal dentate gyrus (DG), while MEC provides the majority of input to the inferior blade [87]. Granule cell populations in the two DG blades are differentially affected by SD, with the inferior blade's activity being selectively suppressed [50], and inferior blade granule cells selectively undergoing dendritic spine loss [88]. Such findings are consistent with a scenario in which input to superior blade (from LEC) is heightened by disinhibition of the LEC network, while input to the inferior blade (from MEC) is either unaffected or suppressed. At the same time, we have recently demonstrated that SD selectively activates SST+ interneuron populations residing in the DG itself [18], which in turn provide stronger inhibition of the inferior blade than the superior blade [23]. Because these different SD-driven processes culminate in selective suppression of context-encoding engram neuron populations within the inferior blade in the hours following CFC [50], the result is disruption of CFM consolidation when animals are sleep deprived.

Previous findings from our lab have suggested that neocortical SST+ interneurons are much more modestly affected by SD than their hippocampal counterparts [22]. Here we show that when SD follows learning, the structure of EC SST+ interneurons, particularly those in the LEC, are dramatically changed. Together these findings suggest profound heterogeneity in the response of SST+ interneurons in different brain regions to sleep loss. Critically, SST+ interneuron populations in other neocortical structures are also selectively activated during SD, and have been implicated in generating the homeostatic change in NREM slow-waves following SD [19,20]. Thus, the heterogeneity of neocortical interneuron responses to SD, and the functional consequences of these SD responses, warrants further investigation.

Sleep loss affects millions of people around the world and has negative outcomes on cognitive functioning. In the United States, lack of sleep has been declared a public health crisis, with nearly a third of adults reporting less than 6 h of sleep per night [89]. Our data highlight selective effects of post-learning sleep loss on SST+ interneurons in EC - a structure essential for cognition. Altered SST+ interneuron function has been implicated in the progression of neurodegenerative and psychiatric disorders such as Alzheimer's disease, bipolar disorder, and schizophrenia [7,14-17]. In all these diseases, disruptions to sleep typically present before alterations to cognition and/or

behavior. Understanding how SD alters the structure, connectivity, and function of SST+ interneurons should provide mechanistic insights for understanding and treating these disorders.

Figure legends:

Figure 1. Brainbow AAV labeling of EC SST+ interneurons, and behavior during post-CFC sleep or SD. (**A, *left***) Mice were virally transduced with Cre recombinase-dependent Brainbow 3.0 in either bilateral MEC or bilateral LEC underwent CFC followed by 6 h of *ad lib* sleep or SD prior to perfusion. (**A, *right***) Neurolucida 360 was used to trace Brainbow-labeled SST+ neurons and classify spine types. Representative 40× images of Brianbow labeling in mouse brains where SST+ interneurons in the LEC and MEC, respectively, were traced using Neurolucida 360. (**B**) Control LEC- and MEC-transduced mice exhibited similar sleep patterns, with both groups sharply increasing the percentage of each hour spent asleep after the first hour post-CFC, and similar sleep bout numbers and durations over the 6-h post-CFC period. (**C**) LEC- and MEC-transduced mice required a similar number of interventions to be kept awake over the course of the 6-h period of post-CFC SD.

Figure 2. Dendritic spine types in LEC and MEC are differentially affected by post-learning SD. (**A**) SD dramatically reduced the proportion of spines with thin morphology in LEC. This change was offset by increased representation of stubby spines after SD. Spine type distributions were largely unaffected in MEC groups after SD. (**B**) Despite a general trend of spine density decreasing after SD, no statistically significant differences in either overall spine density, or thin, mushroom, or stubby spine density in either LEC or MEC. Filopodia spine density in LEC, but MEC, was significantly decreased after SD.

Figure 3. SD dramatically reduces SST+ interneurons' spine size in LEC. (**A**) SD decreased overall spine volume as well as the volume of every spine subtype LEC, except filopodia. (**B**) SD decreased overall spine surface area as well as the spine surface area of every subtype in LEC, except filopodia. (**C**) SD decreased overall spine backbone length as well as the backbone length of thin and stubby spines in the LEC. For cumulative distributions, * and **** indicate $p<0.05$ and $p<0.0001$, respectively, KS test.

Figure 4. SD minimally affects SST+ interneurons' dendritic spine size in MEC. (A) There were no significant changes in spine volume after SD in MEC. (B) There were no significant effects of SD on spine surface area. (C) SD led to a modest, but statistically significant, increase in mushroom spine backbone length in MEC, but did not affect other spine types. For cumulative distributions, * indicates $p<0.05$, KS test.

References:

1. Puentes-Mestril, C., Roach, J., Niethard, N., Zochowski, M., and Aton, S.J. (2019). How rhythms of the sleeping brain tune memory and synaptic plasticity. Sleep *42*, pii: zsz095. 10.1093/sleep/zsz095.
2. Puentes-Mestril, C., and Aton, S.J. (2017). Linking network activity to synaptic plasticity during sleep: hypotheses and recent data. Frontiers in Neural Circuits *11*, doi: 10.3389/fncir.2017.00061.
3. Diekelmann, S., and Born, J. (2010). The memory function of sleep. Nat Rev Neurosci *11*, 114-126.
4. Abel, T., Havekes, R., Saletin, J.M., and Walker, M.P. (2013). Sleep, plasticity and memory from molecules to whole-brain networks. Curr Biol *23*, R774-788.
5. Walker, M.P., and Stickgold, R. (2004). Sleep-dependent learning and memory consolidation. Neuron *44*, 121-133.
6. Sabia, S., Fayosse, A., Dumurgier, J., van Hees, V.T., Paquet, C., Sommerlad, A., Kivimaki, M., Dugravot, A., and Singh-Manoux, A. (2021). Association of sleep duration in middle and old age with incidence of dementia. Nat Commun *12*, 2289.
7. Zhang, Y., Quinones, G.M., and Ferrarelli, F. (2020). Sleep spindle and slow wave abnormalities in schizophrenia and other psychotic disorders: Recent findings and future directions Schizophr Res *221*, 29-36.
8. Harvey, A., Talbot, L., and Gershon, A. (2009). Sleep Disturbance in Bipolar Disorder Across the Lifespan. Clin Psychol (New York) *16*, 156-166.
9. Gerstenberg, M., Furrer, M., Tesler, N., Franscini, M., Walitza, S., and Huber, R. (2020). Reduced sleep spindle density in adolescent patients with early-onset schizophrenia compared to major depressive disorder and healthy controls Schizophr Res *221*, 20-28.
10. Manoach, D.S., Demanuele, C., Wamsley, E.J., Vangel, M., Montrose, D.M., Miewald, J., Kupfer, D., Buysse, D., Stickgold, R., and Keshavan, M.S. (2014). Sleep spindle deficits in antipsychotic-naïve early course schizophrenia and in non-psychotic first-degree relatives. Front Hum Neurosci *8*.
11. Ohara, T., Honda, T., Hata, J., Yoshida, D., Mukai, N., Hirakawa, Y., Shibata, M., Kishimoto, H., Kitazono, T., Kanba, S., and Ninomiya, T. (2018). Association Between Daily Sleep Duration and Risk of Dementia and Mortality in a Japanese Community. J Am Geriatr Soc *66*.
12. Latreille, V., Carrier, J., Lafortune, M., Postuma, R.B., Bertrand, J.A., Panisset, M., Chouinard, S., and Gagnon, J.F. (2015). Sleep spindles in Parkinson's disease may predict the development of dementia. Neurobiol Aging *36*, 1083-1090.
13. Gottesmann, C., and Gottesman, I. (2007). The neurobiological characteristics of rapid eye movement (REM) sleep are candidate endophenotypes of depression, schizophrenia, mental retardation and dementia. Progress in Neurobiology *81*, 237-250.
14. Gabitto, M., Travaglini, J., and Rachleff, V. (2024). Integrated multimodal cell atlas of Alzheimer's disease. Nat Neurosci. https://doi.org/10.1038/s41593-024-01774-5.
15. Dienel, S., Dowling, K., Barile, Z., Bazmi, H., Liu, A., Vespoli, J., Fish, K., and Lewis, D.A. (2023). Diagnostic Specificity and Association With Cognition of Molecular Alterations in Prefrontal Somatostatin Neurons in Schizophrenia. JAMA Psychiatry *80*, 1235-1245.
16. Konradi, C., Yang, C.K., Zimmerman, E.I., Lohmann, K.M., Gresch, P., Pantazopoulos, H., Berretta, S., and Heckers, S. (2011). Hippocampal interneurons are abnormal in schizophrenia Schizophr Res *131*, 165-173.
17. Wang, A., Lohmann, K.M., Yang, C., Zimmerman, E.I., Pantazopoulos, H., Herring, N., Berretta, S., Heckers, S., and Konradi, C. (2011). Bipolar disorder type 1 and

schizophrenia are accompanied by decreased density of parvalbumin- and somatostatin-positive interneurons in the parahippocampal region. . Acta Neuropathol *122*, 615-626.
18. Delorme, J., Wang, L., Roig Kuhn, F., Kodoth, V., Ma, J., Martinez, J.D., Raven, F., Toth, B.A., Balendran, V., Vega Medina, A., et al. (2021). Sleep loss drives acetylcholine- and somatostatin interneuron-mediated gating of hippocampal activity, to inhibit memory consolidation. Proc Natl Acad Sci USA *118*.
19. Funk, C.M., Peelman, K., Bellesi, M., Marshall, W., Cirelli, C., and Tononi, G. (2017). Role of Somatostatin-Positive Cortical Interneurons in the Generation of Sleep Slow Waves. J Neurosci *37*, 9132-9148.
20. Tossell, K., Yu, X., Giannos, P., Anuncibay Soto, B., Nollet, M., Yustos, R., Miracdca, G., Vicente, M., Miao, A., Hsieh, B., et al. (2023). Somatostatin neurons in prefrontal cortex initiate sleep-preparatory behavior and sleep via the preoptic and lateral hypothalamus. Nat Neurosci *26*, 1805-1819.
21. Delorme, J.E., Kodoth, V., and Aton, S.J. (2019). Sleep loss disrupts Arc expression in dentate gyrus neurons. Neurobiol Learn Mem *160*, 73-82.
22. Raven, F., Vega Medina, A., Schmidt, K., He, A., Vankampen, A., Balendran, V., and Aton, S. (2025). Brief sleep disruption alters synaptic structures among hippocampal and neocortical somatostatin-expressing interneurons. Sleep *2025*, zsaf064. 10.1101/2024.07.22.604591.
23. Raven, F., Vankampen, A., He, A., and Aton, S. (2025). Dentate gyrus network regulation by somatostatin- and parvalbumin-expressing interneurons differentially impacts hippocampal spatial memory processing. bioRxiv, 07.23.666335.
24. Takehara-Nishiuchi, K. (2014). Entorhinal cortex and consolidated memory. . Neurosci Res *84*, 27-33.
25. Knierim, J., Neunuebel, J., and Deshmukh, S. (2014). Functional correlates of the lateral and medial entorhinal cortex: objects, path integration and local–global reference frames. Philos Trans R Soc London B Biol Sci *369*, 20130369.
26. Tsoi, S., Oncul, M., Svahn, E., Roberston, M., Bogdanowicz, Z., McClure, C., and Surmeli, G. (2022). Telencephalic outputs from the medial entorhinal cortex are copied directly to the hippocampus eLife *11*, e73162.
27. Przy, R., Wade, M., Welter, P., Brocardo, P., and Christie, B.R. (2025). Lateral Thinking: Exploring the Lateral Entorhinal Cortex Projections to the Hippocampus in the Rodent Brain. J Comp Neurol *533*, e70069.
28. Knierim, J.J. (2015). From the GPS to HM: Place cells, grid cells, and memory Hippocampus *25*, 719-725.
29. Basu, J., and Siegelbaum, S. (2015). The Corticohippocampal Circuit, Synaptic Plasticity, and Memory. Cold Spring Harbor Perspect Biol *7*, a021733.
30. Danieli, K., Guyon, A., and Bethus, I. (2023). Episodic Memory formation: A review of complex Hippocampus input pathways. Prog Neuropsychopharmacol Biol Psychiatry *126*, 110757.
31. Dubanet, O., and Higley, M.J. (2024). Retrosplenial inputs drive visual representations in the medial entorhinal cortex Cell Rep *43*, 114470.
32. Kononenko, N., and Witter, M.P. (2012). Presubiculum layer III conveys retrosplenial input to the medial entorhinal cortex. . Hippocampus *22*, 881-895.
33. Wilson, D., Watanabe, S., Milner, H., and Ainge, J. (2013). Lateral entorhinal cortex is necessary for associative but not nonassociative recognition memory. Hippocampus *23*, 1280-1290.
34. Basu, J., and Nagel, K. (2024). Neural circuits for goal-directed navigation across species. . Trends Neurosci *47*, 904-917.
35. Tsao, A., Sugar, J., Lu, L., Wang, C., Knierim, J.J., Moser, M., and Moser, E. (2018). Integrating time from experience in the lateral entorhinal cortex. . Nature *561*, 57-62.

36. Heckman, P.R.A., Roig-Kuhn, F., Meerlo, P., and Havekes, R. (2020). A brief period of sleep deprivation negatively impacts the acquisition, consolidation, and retrieval of object-location memories. Neurobiol Learn Mem *175*.
37. Graves, L.A., Heller, E.A., Pack, A.I., and Abel, T. (2003). Sleep deprivation selectively impairs memory consolidation for contextual fear conditioning. Learn. Mem. *10*, 168-176.
38. Vecsey, C.G., Baillie, G.S., Jaganath, D., Havekes, R., Daniels, A., Wimmer, M., Huang, T., Brown, K.M., Li, X.Y., Descalzi, G., et al. (2009). Sleep deprivation impairs cAMP signalling in the hippocampus. Nature *461*, 1122-1125.
39. Ognjanovski, N., Broussard, C., Zochowski, M., and Aton, S.J. (2018). Hippocampal Network Oscillations Rescue Memory Consolidation Deficits Caused by Sleep Loss. Cereb. Cortex *28*, 3711-3723. 10.1093/cercor/bhy174.
40. Delorme, J., Wang, L., Kodoth, V., Wang, Y., Ma, J., Jiang, S., and Aton, S.J. (2021). Hippocampal neurons' cytosolic and membrane-bound ribosomal transcript profiles are differentially regulated by learning and subsequent sleep. Proc Natl Acad Sci USA *118*.
41. Yang, G., Lai, C.S., Cichon, J., Ma, L., Li, W., and Gan, W.B. (2014). Sleep promotes branch-specific formation of dendritic spines after learning. Science *344*, 1173-1178.
42. Martinez, J.D., Donnelly, M.J., Popke, D.S., Torres, D., Wilson, L.G., Brancaleone, W.P., Sheskey, S., Lin, C.-M., Clawson, B.C., Jiang, S., and Aton, S.J. (2023). Enriched binocular experience followed by sleep optimally restores binocular visual cortical responses in a mouse model of amblyopia. Communications Biology *6*, 408.
43. Clawson, B.C., Durkin, J., Suresh, A.K., Pickup, E.J., Broussard, C.G., and Aton, S.J. (2018). Sleep Promotes, and Sleep Loss Inhibits, Selective Changes in Firing Rate, Response Properties and Functional Connectivity of Primary Visual Cortex Neurons. Frontiers in Systems Neuroscience *12*, 40. doi: 10.3389/fnsys.2018.00040.
44. Clawson, B.C., Pickup, E.J., Enseng, A., Geneseo, L., Shaver, J., Gonzalez-Amoretti, J., Zhao, M., York, A.K., Kuhn, F.R., Swift, K.M., et al. (2021). Causal role for sleep-dependent reactivation of learning-activated sensory ensembles for fear memory consolidation. Nat Communications *12*.
45. Bridi, M.C.D., Aton, S.J., Seibt, J., Renouard, L., Coleman, T., and Frank , M.G. (2015). Rapid eye movement sleep promotes cortical plasticity in the developing brain. Science Advances *1*, 1-8.
46. Aton, S.J., Suresh, A., Broussard, C., and Frank, M.G. (2014). Sleep promotes cortical response potentiation following visual experience. Sleep *37*, 1163-1170.
47. Aton, S.J., Broussard, C., Dumoulin, M., Seibt, J., Watson, A., Coleman, T., and Frank , M.G. (2013). Visual experience and subsequent sleep induce sequential plastic changes in putative inhibitory and excitatory cortical neurons. Proc Natl Acad Sci U S A *110*, 3101-3106.
48. Aton, S.J., Seibt, J., Dumoulin, M., Jha, S.K., Steinmetz, N., Coleman, T., Naidoo, N., and Frank, M.G. (2009). Mechanisms of sleep-dependent consolidation of cortical plasticity. Neuron *61*, 454-466.
49. Zhou, Y., Lai, C.S.W., Bai, Y., Li, W., Zhou, R., Yang, G., Frank, M.G., and Gan, W.-B. (2020). REM sleep promotes experience-dependent dendritic spine elimination in the mouse cortex Nat Communications *11*.
50. Wang, L., Park, L., Wu, W., King, D., Vega-Medina, A., Raven, F., Martinez, J., Enseng, A., McDonald, K., Yang, Z., et al. (2024). Sleep-dependent engram reactivation during hippocampal memory consolidation associated with subregion-specific biosynthetic changes. iScience *27*, 109408. 10.1016/j.isci.2024.109408
51. Puentes-Mestril, C., Delorme, J., Wang, L., Donnelly, M., Popke, D., Jiang, S., and Aton, S.J. (2021). Sleep loss drives brain region- and cell type-specific alterations in ribosome-associated transcripts involved in synaptic plasticity and cellular timekeeping. J Neurosci *41*, 5386-5398.

52. Cai, D., Cohen, K.B., Luo, T., Lichtman, J.W., and Sanes, J.R. (2013). Improved tools for the Brainbow toolbox. Nature Methods *10*, 540-547.
53. Martinez, J.D., Wilson, L.G., Peterson, K.G., Brancaleone, W.P., Popke, D.S., Caicedo Garzon, V., Perez Tramble, R.E., Donnelly, M.J., Torres, D., Mendez Ortega, S.L., et al. (2024). Hypnotic treatment reverses NREM sleep disruption and EEG desynchronization in a mouse model of Fragile X syndrome to rescue memory consolidation deficits. . Cell Rep *43*, 114266.
54. Martinez, J.D., Brancaleone, W.P., Peterson, K.G., Wilson, L.G., and Aton, S.J. (2023). Atypical hypnotic compound ML297 restores sleep architecture immediately following emotionally valenced learning, to promote memory consolidation and hippocampal network activation during recall Sleep *46*, zsac301.
55. Djurisic, M., Vidal, G., Mann, M., Aharon, A., Kim, T.-K., Ferrao Santos, A., Zuo, Y., Hubener, M., and Shatz, C. (2013). PirB regulates a structural substrate for cortical plasticity. Proc Natl Acad Sci U S A *110*, 20771-20776.
56. Runge, K., Cardoso, C., and de Chevigny, A. (2020). Dendritic Spine Plasticity: Function and Mechanisms. Front Synaptic Neurosci *12*, 36.
57. Hering, H., and Sheng, M. (2001). Dentritic spines : structure, dynamics and regulation. Nat Rev Neurosci *2*, 880-888.
58. Rodriguez, A., Ehlenberger, D., Dickstein, D., Hof, P., and Wearne, S.L. (2008). Automated Three-Dimensional Detection and Shape Classification of Dendritic Spines from Fluorescence Microscopy Images. PLoS One *3*, e1997.
59. Bourne, J., and Harris, K. (2007). Do thin spines learn to be mushroom spines that remember? . Curr Opin Neurobiol *17*, 381-386.
60. Tonnesen, J., Katona, G., Rozsa, B., and Nagerl, U. (2014). Spine neck plasticity regulates compartmentalization of synapses. . Nat Neurosci *17*, 678-685.
61. de Vivo, L., Bellesi, M., Marshall, W., Bushong, E.A., Ellisman, H., Tononi, G., and Cirelli, C. (2017). Ultrastructural evidence for synaptic scaling across the wake/sleep cycle. Science *355*, 507-510.
62. de Vivo, L., Nelson, A.B., Bellesi, M., Noguti, J., Tononi, G., and Cirelli, C. (2016). Loss of sleep affects the ultrastructure of pyramidal neurons in the adolescent mouse frontal cortex. . Sleep *39*, 861-874.
63. Spano, G.M., Banningh, S.W., Marshall, W., de Vivo, L., Bellesi, M., Loschky, S.S., Tononi, G., and Cirelli, C. (2019). Sleep Deprivation by Exposure to Novel Objects Increases Synapse Density and Axon-Spine Interface in the Hippocampal CA1 Region of Adolescent Mice. J Neurosci *39*, 6613-6625.
64. Borczyk, M., Sliwinska, M., Caly, A., Bernas, T., and Radwanska, K. (2019). Neuronal plasticity affects correlation between the size of dendritic spine and its postsynaptic density. Sci Rep *9*, 1693.
65. Hotulainen, P., and Hoogenraad, C. (2010). Actin in dendritic spines: connecting dynamics to function. J Cell Biol *189*, 619-629.
66. Chidabaram, S., Rathipriya, A., Bolla, S., Bhad, A., Ray, B., Mahalakshmi, A., Manivasagam, T., Thenmozhi, A., Essa, M., Guillemin, G., et al. (2019). Dendritic spines: Revisiting the physiological role. Prog Neuropsychopharmacol Biol Psychiatry *92*, 161-193.
67. Bosch, M., Castro, J., Saneyoshi, T., Matsuno, H., Sur, M., and Hayashi, Y. (2014). Structural and molecular remodeling of dendritic spine substructures during long-term potentiation. Neuron *82*, 444-459.
68. Attardo, A., Fitzgerald, J.E., and Schnitzer, M.J. (2015). Impermanence of dendritic spines in live adult CA1 hippocampus. Nature *523*, 592-596.

69. Holtmaat, A., Trachtenberg, J., Wilbrecht, L., Shepherd, G., Zhang, X., Knott, G., and Svoboda, K. (2005). Transient and persistent dendritic spines in the neocortex in vivo Neuron *45*, 279-291.
70. Yang, G., Pan, F., and Gan, W. (2009). Stably maintained dendritic spines are associated with lifelong memories. . Nature *462*, 920-924.
71. Fiala, J., Feinberg, M., Popov, V., and Harris, K. (1998). Synaptogenesis via dendritic filopodia in developing hippocampal area CA1. . J Neurosci *18*, 8900-8911.
72. Adler, A., Lai, C., Yang, G., Geron, E., Bai, Y., and Gan, W.-B. (2021). Sleep promotes the formation of dendritic filopodia and spines near learning-inactive existing spines Proc Natl Acad Sci U S A *118*, e2114856118.
73. Trachtenberg, J.T., Chen, B., Knott, G., Feng, G., Sanes, J.R., Welker, E., and Svoboda, K. (2002). Long-term in vivo imaging of experience-dependent synaptic plasticity in adult cortex. Nature *420*, 788-794.
74. Hasegawa, S., Sakuragi, S., Tominaga-Yoshino, K., and Ogura, A. (2015). Dendritic spine dynamics leading to spine elimination after repeated inductions of LTD. Scientific Reports *5*, 7707.
75. Harris, K., Jensen, F., and Tsao, B. (1992). Three-dimensional structure of dendritic spines and synapses in rat hippocampus (CA1) at postnatal day 15 and adult ages: implications for the maturation of synaptic physiology and long-term potentiation. . J Neurosci *12*, 2685-2705.
76. Scheuss, V., and Bonhoeffer, T. (2014). Function of dendritic spines on hippocampal inhibitory neurons Cereb Cortex *24*, 3142-3153.
77. Haist, F., Bowden Gore, J., and Mao, H. (2001). Consolidation of human memory over decades revealed by functional magnetic resonance imaging. Nat Neurosci *4*, 1139-1145.
78. Sparta, D., Smithuis, J., Stamatakis, A., Jennings, J., Kantak, P., Ung, R., and Stuber, G. (2014). Inhibition of projections from the basolateral amygdala to the entorhinal cortex disrupts the acquisition of contextual fear Front Behav Neurosci *8*, 129.
79. Lu, L., Leutgeb, J., Tsao, A., Henriksen, E., Leutgeb, S., Barnes, C.A., Witter, M.P., Moser, M., and Moser, E. (2013). Impaired hippocampal rate coding after lesions of the lateral entorhinal cortex. Nat Neurosci *16*, 1085-1093.
80. Heimly Brun, V., Leutgeb, S., Wu, H.-Q., Schwartz, R., Witter, M.P., Moser, E., and Moser, M. (2008). Impaired spatial representation in CA1 after lesion of direct input from entorhinal cortex Neuron *57*, 290-302.
81. Zhang, S., Ye, J., Miao, C., Tsao, A., Cerniauskas, I., Ledergerber, D., Moser, M., and Moser, E. (2013). Optogenetic dissection of entorhinal-hippocampal functional connectivity. . Science *340*, 1232627.
82. Miao, C., Cao, Q., Moser, M., and Moser, E. (2017). Parvalbumin and Somatostatin Interneurons Control Different Space-Coding Networks in the Medial Entorhinal Cortex Cell *171*, 507-521.
83. Kang, M., and Han, J.-H. (2021). Optogenetic inhibition of medial entorhinal cortex inputs to the hippocampus during a short period of time right after learning disrupts contextual fear memory formation. Mol Brain *14*, 2.
84. O'Neill, J., Boccara, C., Stella, F., Schoenenberger, P., and Csicsivari, J. (2017). Superficial layers of the medial entorhinal cortex replay independently of the hippocampus Science *355*, 184-188.
85. Tozzi, F., Gugielmo, S., Paraciani, C., van den Oever, M.C., Mainardi, M., Catteano, A., and Origlia, N. (2024). Involvement of a lateral entorhinal cortex engram in episodic-like memory recall. Cell Rep *43*, 114795.
86. Xie, M., Li, C., He, C., Yang, L., Tan, G., Yan, J.-Z., Wang, J., and Hu, Z. (2016). Short-term sleep deprivation disrupts the molecular composition of ionotropic glutamate

receptors in entorhinal cortex and impairs the rat spatial reference memory Behav Brain Res *300*, 70-76.
87. Witter, M.P. (2007). The perforant path: projections from the entrhinal cortex to the dentate gyrus. Prog Brain Res *163*, 43-61.
88. Raven, F., Meerlo, P., Van der Zee, E.A., Abel, T., and Havekes, R. (2019). A brief period of sleep deprivation causes spine loss in the dentate gyrus of mice. Neurobiol Learn Mem *160*, 83-90.
89. Barnes, C., and Drake, C. (2015). Prioritizing Sleep Health: Public Health Policy Recommendations. . Perspect Psychol Sci *10*, 733-737.

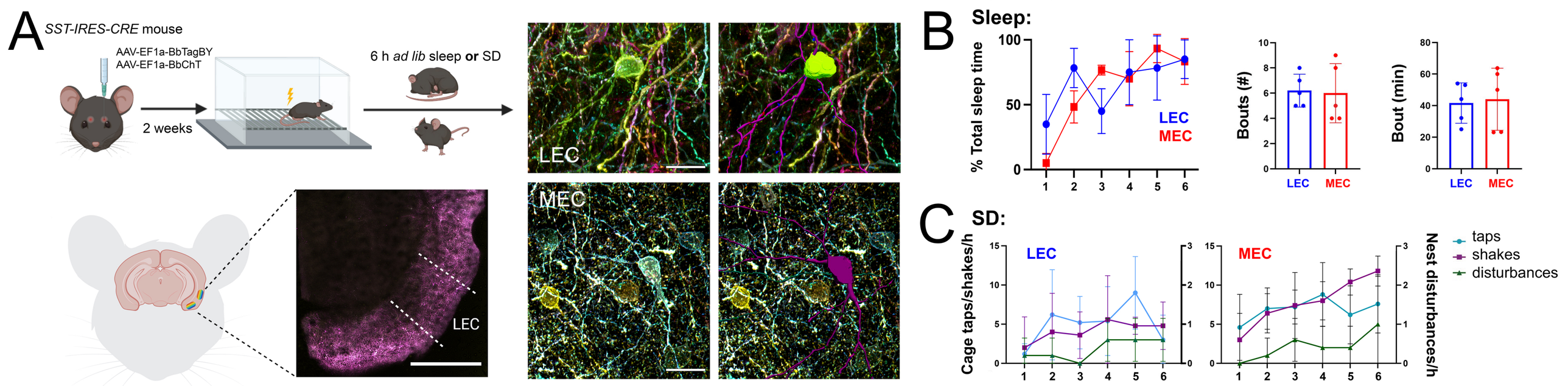
A
SST-IRES-CRE mouse
AAV-EF1a-BbTagBY
AAV-EF1a-BbChT
2 weeks
6 h ad lib sleep or SD
LEC
MEC
LEC
B
Sleep:
% Total sleep time
LEC
MEC
Bouts (#)
Bout (min)
C
SD:
Cage taps/shakes/h
Nest disturbances/h
taps
shakes
disturbances

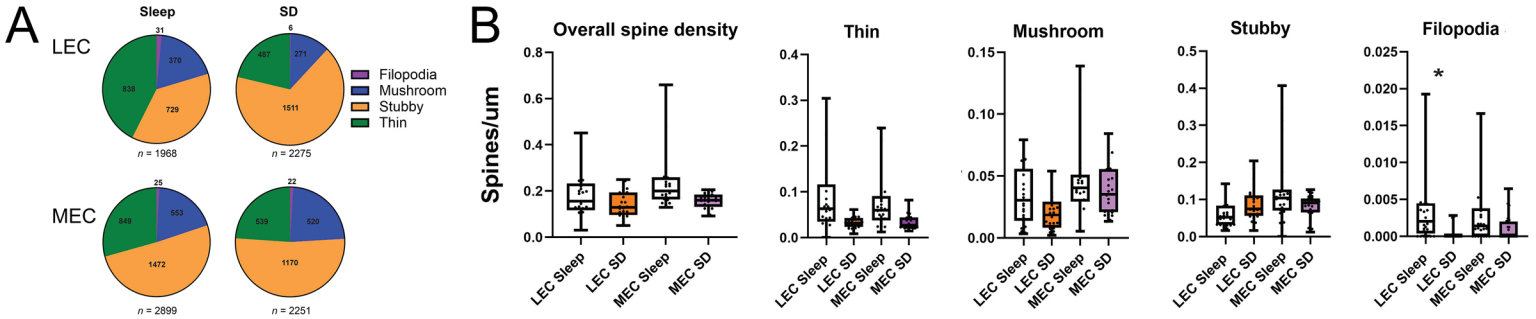
A
Sleep
SD
LEC
MEC
31
370
729
838
n = 1968
6
271
1511
467
n = 2275
25
553
1472
849
n = 2899
22
520
1170
539
n = 2251
Filopodia
Mushroom
Stubby
Thin
B
Spines/um
Overall spine density
Thin
Mushroom
Stubby
Filopodia
*
LEC Sleep
LEC SD
MEC Sleep
MEC SD

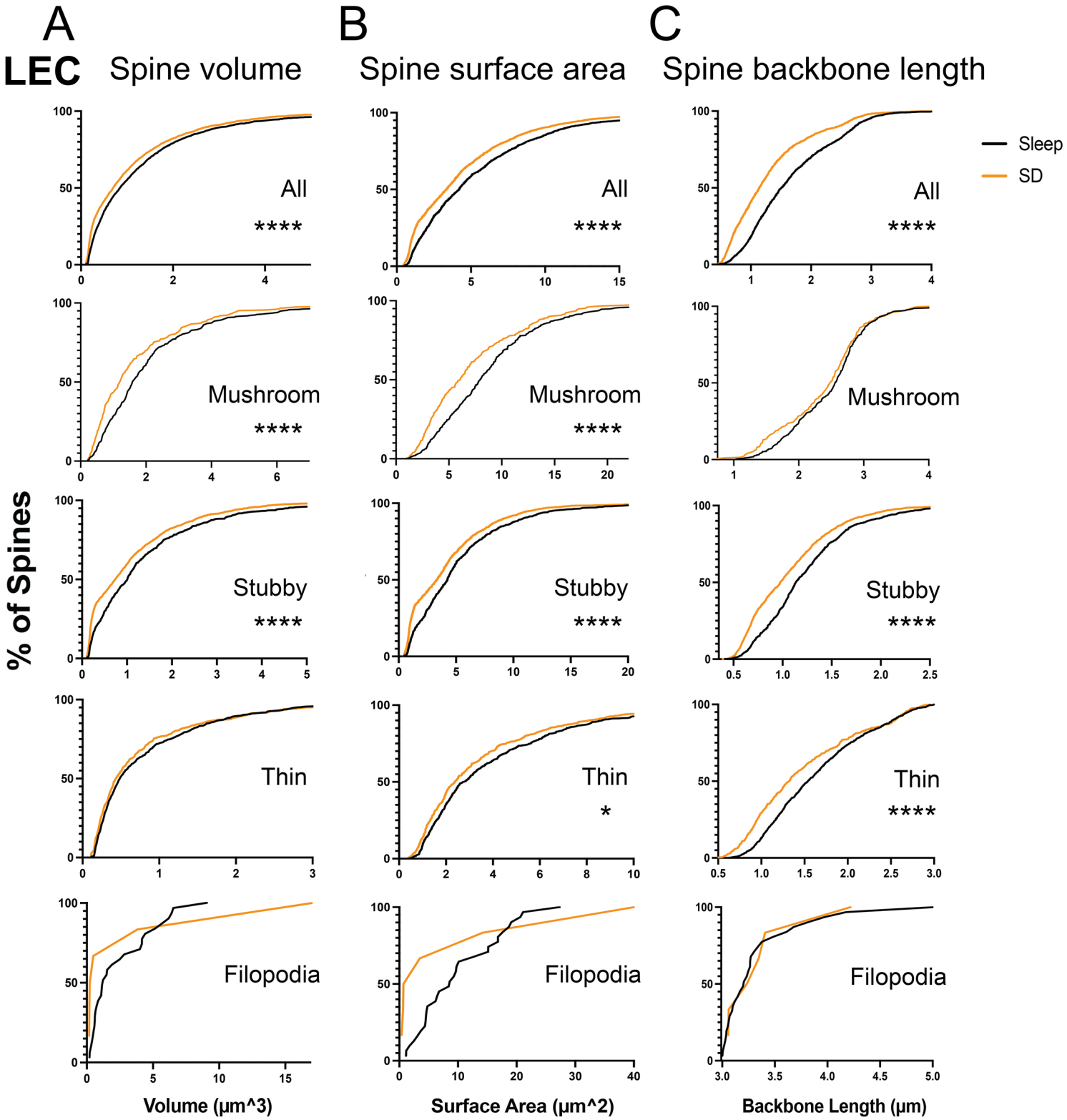
A
B
C
LEC
Spine volume
Spine surface area
Spine backbone length
Sleep
SD
% of Spines
All
****
Mushroom
****
Stubby
****
Thin
Thin
*
Thin
****
Filopodia
Volume (µm^3)
Surface Area (µm^2)
Backbone Length (µm)

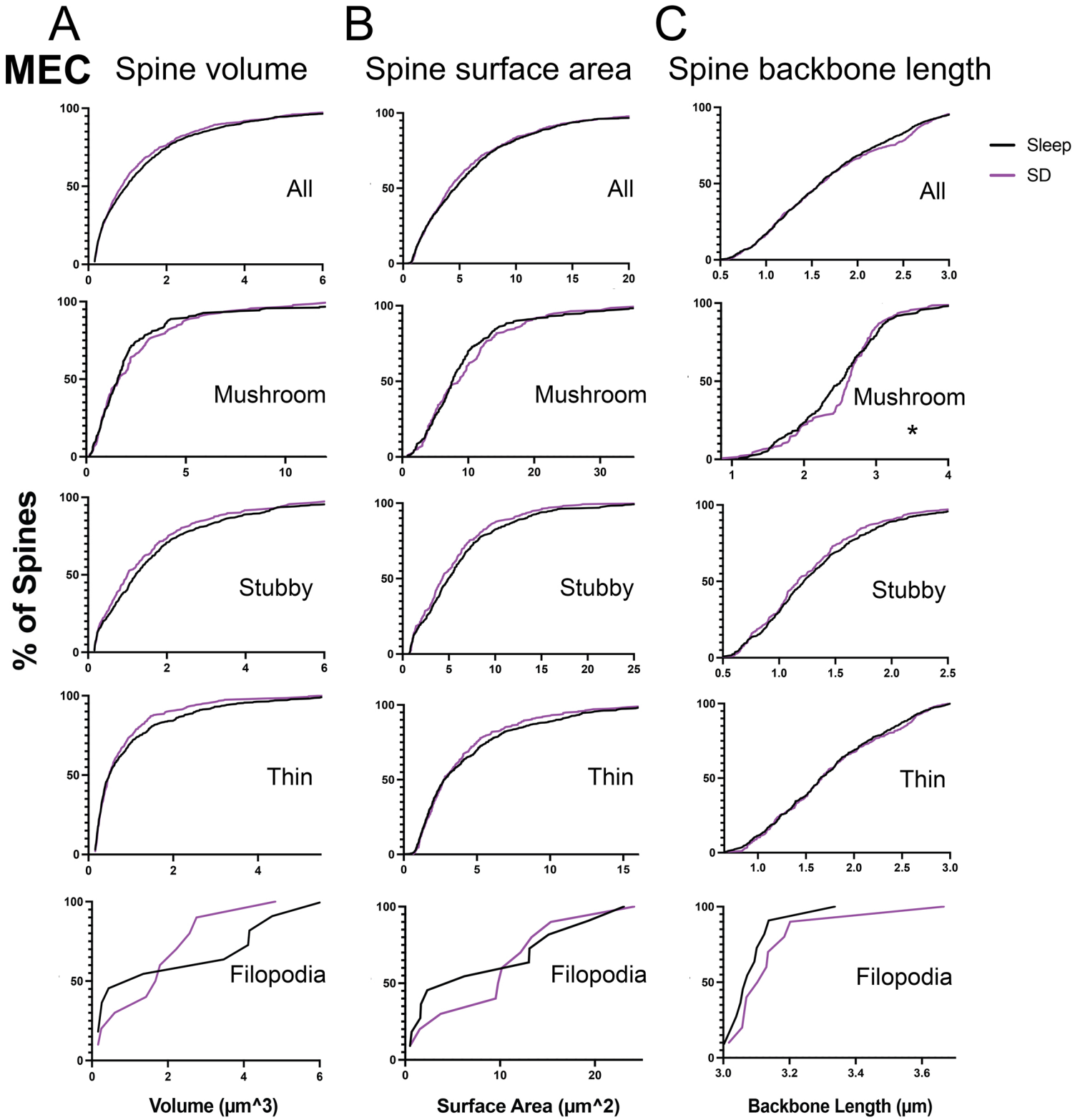
A
MEC
Spine volume
B
Spine surface area
C
Spine backbone length
Sleep
SD
All
Mushroom
Stubby
Thin
Filopodia
*
% of Spines
Volume (µm^3)
Surface Area (µm^2)
Backbone Length (µm)